PROCEEDINGS OF THE ROYAL SOCIETY A

rspa.royalsocietypublishing.org

Research

Cite this article: Carusotto I. 2014 Superfluid light in bulk nonlinear media. *Proc. R. Soc. A* **470**: 20140320.
http://dx.doi.org/10.1098/rspa.2014.0320

Received: 17 April 2014
Accepted: 11 June 2014

Subject Areas:
optics, quantum physics, statistical physics

Keywords:
superfluidity, light, nonlinear optics

Author for correspondence:
Iacopo Carusotto
e-mail: carusott@science.unitn.it

Superfluid light in bulk nonlinear media

Iacopo Carusotto

INO-CNR BEC Center and Dipartimento di Fisica, Università di Trento, via Sommarive 14, Povo 38123, Italy

We review how the paraxial approximation naturally leads to a hydrodynamic description of light propagation in a bulk Kerr nonlinear medium in terms of a wave equation analogous to the Gross–Pitaevskii equation for the order parameter of a superfluid. The main features of the many-body collective dynamics of the fluid of light in this propagating geometry are discussed: generation and observation of Bogoliubov sound waves in the fluid of light is first described. Experimentally accessible manifestations of superfluidity are then highlighted. Perspectives in view of realizing analogue models of gravity are finally given.

1. Introduction

Experimental studies of the so-called fluids of light are opening new perspectives to the field of many-body physics, as they allow unprecedented control and flexibility in the generation, manipulation and control of Bose fluids [1]. So far, a number of striking experimental observations have been performed using a semiconductor planar microcavity architecture, including the demonstration of a superfluid flow [2] and of the hydrodynamic nucleation of solitons and quantized vortices [3–5].

An alternative platform for studying many body physics in fluids of light consists of a bulk nonlinear medium showing an intensity-dependent refractive index: under the paraxial approximation, the propagation of monochromatic light can be described in terms of a Gross–Pitaevskii equation (GPE) for the order parameter, in our case the electric field amplitude of the monochromatic beam. Even though experimental studies of this system have started much earlier, up to now only a little attention has been devoted to hydrodynamic and superfluid features. Among the most remarkable exceptions, we may mention the recent works [6–13].

Royal Society Publishing

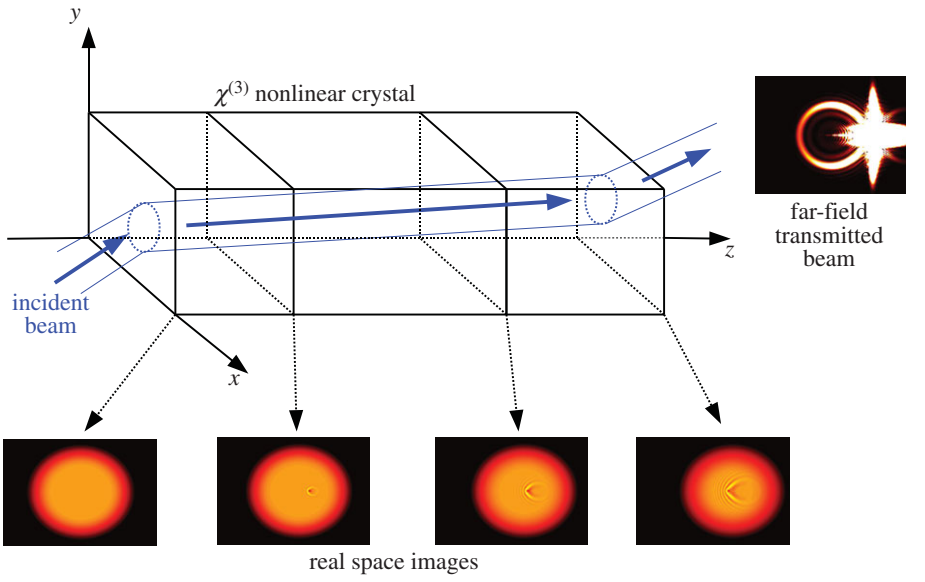

Figure 1. Sketch of the experimental configuration under investigation in this work. The small panels in the bottom of the figure show an illustrative example of a series of intensity profiles after different distances of propagation along the crystal. The small panel on the right shows an example of far-field transmitted intensity profile. (Online version in colour.)

This short article reports an application of superfluid hydrodynamics concepts to the theoretical study of classical light propagation in bulk nonlinear crystals. Section 2 describes the system under consideration and reviews the main steps of the derivation of the well-known paraxial wave equation in a Kerr nonlinear medium: in contrast to the microcavity architecture used in the experiments of [2–5], where the temporal dynamics of the fluid of light is described by a driven-dissipative equation, paraxial propagation in a bulk nonlinear crystal is described by a fully conservative GPE and the initial density and flow speed of the light fluid are directly controlled by the intensity and the angle of incidence of the incident beam. Schemes where a second laser beam is used to generate and observe collective excitations in the fluid of light are discussed in §3. The interaction of a flowing fluid of light with a localized defect is studied in §4: signatures of superfluid behavior are highlighted, as well as the main mechanisms for breaking superfluidity. Perspectives in view of using superfluids of light for experimental studies of analogue models of gravity are finally outlined in §5. The conclusion is drawn in §6.

2. The model

The system we are considering is sketched in figure 1: a monochromatic wave of frequency ω_0 is incident on a crystal of linear dielectric constant ϵ and Kerr optical nonlinearity $\chi^{(3)}$. The front interface of the crystal is assumed to lie on the (x, y) plane, while the incident beam is assumed to propagate close to the longitudinal direction z.

Neglecting for simplicity polarization degrees of freedom, the propagation equation of light in the crystal can be described by the usual nonlinear wave equation

$$\partial_z^2 E(\mathbf{r}_\perp, z) + \nabla_\perp^2 E(\mathbf{r}_\perp, z) + \frac{\omega_0^2}{c^2}[\epsilon + \delta\epsilon(\mathbf{r}_\perp, z) + \chi^{(3)}|E(\mathbf{r}_\perp, z)|^2]E(\mathbf{r}_\perp, z), \tag{2.1}$$

for the complex amplitude $E(\mathbf{r}_\perp, z)$ of the monochromatic field. The $\nabla_\perp$ gradient is taken along the transverse $\mathbf{r}_\perp = (x, y)$ coordinates only. The spatial modulation of the linear dielectric constant $\delta\epsilon(\mathbf{r}_\perp, z)$ is assumed to be slowly varying in space. A further slow modulation of the effective

dieletric constant proportional to the local light intensity is provided by the following term involving the third-order Kerr optical nonlinearity $\chi^{(3)}$ of the medium.

Provided the variation of the field amplitude $E(\mathbf{r}_\perp, z)$ along the transverse plane is slow enough, we can perform the so-called paraxial approximation. In terms of the slowly varying envelope $\mathcal{E}(\mathbf{r}_\perp, z) = E(\mathbf{r}_\perp, z)\,\mathrm{e}^{-\mathrm{i}k_0 z}$, the paraxial approximation is accurate as long as $|\nabla_\perp^2 \mathcal{E}|/k_0^2 \sim |\partial_z \mathcal{E}|/k_0 \ll 1$ with $k_0 = \sqrt{\epsilon}\omega_0/c$. Under this assumption, the second z derivative term can be neglected in the propagation equation for $\mathcal{E}$, which is then written in the form of a nonlinear Schrödinger equation,

$$\mathrm{i}\partial_z \mathcal{E}(\mathbf{r}_\perp, z) = -\frac{1}{2k_0}\nabla_\perp^2 \mathcal{E} - \frac{k_0}{2\epsilon}(\delta\epsilon(\mathbf{r}_\perp, z) + \chi^{(3)}|\mathcal{E}(\mathbf{r}_\perp, z)|^2)\mathcal{E}(\mathbf{r}_\perp, z) \tag{2.2}$$

with a positive effective mass proportional to k_0.

The spatial modulation of the dielectric constant provides an external potential term $V(\mathbf{r}_\perp, z) = -k_0\delta\epsilon(\mathbf{r}_\perp, z)/(2\epsilon)$: higher (lower) refractive index means attractive (repulsive) potential. In experiments, a wide variety of $\delta\epsilon(\mathbf{r}_\perp, z)$ profiles can be generated either in a static way by micro-structuring the physical and chemical properties of the crystal or by dynamically inducing a refractive index modulation with a strong additional laser beam via the optical nonlinearity of the medium, e.g. the photo-refractive one [8]: the power and flexibility of femtosecond laser writing techniques to realize a rich variety of three-dimensional structures is reviewed in [14] and exemplified in [15]. Rich structures such as rotating waveguide arrays can also be generated taking advantage of the complex propagation dynamics of the strong additional laser driving the photo-refractive nonlinearity [16].

The optical nonlinearity gives a photon–photon interaction constant $g = -\chi^{(3)}k_0/2\epsilon$: a focusing $\chi^{(3)} > 0$ (defocusing $\chi^{(3)} < 0$) optical nonlinearity corresponds to an attractive $g < 0$ (repulsive $g > 0$) effective interaction between photons. Throughout this work, we focus our attention on the more stable defocusing $\chi^{(3)} < 0$ case giving repulsive $g > 0$ interactions. We also restrict our attention to the case of a weak nonlinearity, where the observed refractive index modulation is the result of the collective interaction of a huge number of photons.

In a typical experiment, a monochromatic laser beam is shown on the front surface of the crystal: the amplitude profile $E_0(\mathbf{r}_\perp)$ of the incident beam on the front surface $z = 0$ fixes the initial condition $\mathcal{E}(\mathbf{r}_\perp, z = 0) = E_0(\mathbf{r}_\perp)$. For a plane wave incident beam at an angle ϕ to the z-axis, conservation of the transverse wavevector along the (x, y) plane $k_\perp^{\mathrm{inc}} = (\omega_0/c)\sin\phi$ fixes the transverse flow speed to

$$v = \epsilon^{-1/2}\sin\phi \simeq \epsilon^{-1/2}\phi, \tag{2.3}$$

where the last approximate equality holds within the paraxial approximation. The Schrödinger-like equation (2.2) then describes how the transverse profile of the laser beam evolves during propagation along the nonlinear crystal. The interpretation of this optical phenomenon in terms of a *fluid of light* stems from the formal analogy of this equation with the GPE for the order parameter of a superfluid or, equivalently, the macroscopic wave function of a dilute Bose–Einstein condensate [17].

Before proceeding, it is however crucial to stress that while the standard GPE for superfluid helium or ultracold atomic clouds describes the evolution of the macroscopic wave function in real time, equation (2.2) refers to a propagation in space: a space–time mapping is therefore understood when speaking about fluid of light in the present context. This seemingly minor issue will have profound consequences when one tries to build from (2.2) a fully quantum field theory accounting also for the corpuscular nature of light. This task is of crucial importance to describe the strong nonlinearity case, where just a few photons are able to produce sizable nonlinear effects. First experimental studies of this novel regime have been recently reported using coherently a gas of dressed atoms in the so-called Rydberg–EIT regime [18].

3. Sound waves in the fluid of light

Transposing to the present optical context, the Bogoliubov theory of weak perturbations on top of a weakly interacting Bose condensate [17], the dispersion of the elementary excitations on top of a spatially uniform fluid of light of density $|E_0|^2$ at rest has the form

$$W_{\rm Bog}(\mathbf{k}_\perp) = \sqrt{\frac{k_\perp^2}{2k_0}\left(\frac{k_\perp^2}{2k_0} - \frac{k_0\chi^{(3)}|E_0|^2}{\epsilon}\right)}. \tag{3.1}$$

Depending on the relative value of the excitation wavevector k as compared to the so-called healing length

$$\xi = \left[-\frac{2\epsilon}{(\chi^{(3)}\,|E_0|^2)}\right]^{1/2} k_0^{-1}, \tag{3.2}$$

two regimes can be identified. Small momentum excitations with $k_\perp\xi \ll 1$ have a sonic dispersion $W_{\rm Bog} \simeq c_{\rm s}|\mathbf{k}|$ with a speed of sound equal to

$$c_{\rm s} = \left[-\frac{\chi^{(3)}|E_0|^2}{2\epsilon}\right]^{1/2} \tag{3.3}$$

and collective nature: physically, they can be understood as phonon waves propagating on top of the light fluid at the speed of sound $c_{\rm s}$. Large momentum excitations with $k_\perp\xi \gg 1$ have instead a parabolic dispersion $W_{\rm Bog} \simeq k_\perp^2/(2k_0)$ and a single-particle character: physically, they can be understood as a particle—a photon—being excited out of the Bose-condensed cloud into the high-momentum state of wavevector $\mathbf{k}_\perp$, where it travels undisturbed through the fluid at high speed. As expected, in the linear optics limit of weak light intensities, one has a vanishing speed of sound $c_{\rm s} \to 0$, a diverging healing length $\xi \to \infty$ and all excitations have a single-particle nature.

Of course, this physics only occurs in the case of a defocusing $\chi^{(3)} < 0$ nonlinearity when the photon–photon interaction is repulsive. In the opposite $\chi^{(3)} > 0$ case, the attractive photon–photon interaction would make the fluid of light unstable against modulational instabilities, which is signalled by the Bogoliubov dispersion $W_{\rm Bog}(\mathbf{k}_\perp)$ becoming imaginary at low wavevectors. In the optical language, this instability for a focusing nonlinearity $\chi^{(3)} > 0$ goes under the name of filamentation of the laser beam.

It is worth noting that, as a consequence of the space–time $t \leftrightarrow z$ mapping underlying the Schrödinger equation (2.2), frequencies $W_{\rm Bog}(\mathbf{k}_\perp)$ are measured in inverse lengths and speeds like v, $c_{\rm s}$ and $v_{\rm gr} = \nabla_{\mathbf{k}} W_{\rm Bog}(\mathbf{k}_\perp)$ are measured in adimensional units, as they have the physical meaning of propagation angles with respect to the z-axis. As the maximum refractive index change that can be achieved before damaging the medium is typically $\delta n_{\rm max} = \chi^{(3)}\,|E_{\rm max}|^2/(2\sqrt{\epsilon}) \ll 1$, both the speed of sound $c_{\rm s} \ll 1$ and the healing length $k_0\xi \gg 1$ are well captured by the paraxial approximation. For convenience, the wavelength $\lambda_0 = 2\pi/k_0$ will be used as a unit of length in all figures.

A simple experiment to characterize the Bogoliubov modes of a fluid of light is to use a strong and wide monochromatic *pump* laser beam of amplitude E_0 to generate the background fluid of light, and then to use a second, weaker *probe* beam at the same frequency ω_0 to create excitations on top of it. This configuration is studied in figure 2: the pump spot is taken to have a wide Gaussian shape and to hit the crystal at normal incidence. The spatially localized perturbation is created by another Gaussian beam with much smaller waist and incident at the centre of the pump spot with a finite incidence angle $\phi_{\rm pr}$. This angle controls the in-plane wavevector of the induced perturbation via the geometric relation $k_\perp^{\rm pr} = (\omega_0/c)\sin\phi_{\rm pr}$.

When the Bogoliubov theory [17] is used to translate the initial condition on the front interface of the crystal into the eigenstates of the propagation dynamics, the photons that are introduced by the probe beam in the $\mathbf{k}_\perp^{\rm pr}$ mode become a superposition of Bogoliubov excitations with opposite momenta $\pm\mathbf{k}_\perp^{\rm pr}$. During propagation, these excitations move with opposite speeds determined by the group velocity $\mathbf{v}_{\rm gr} = \nabla_{\mathbf{k}} W_{\rm Bog}$ evaluated at $\pm\mathbf{k}_\perp^{\rm pr}$. Depending on the value of the $k_\perp^{\rm pr}\xi$

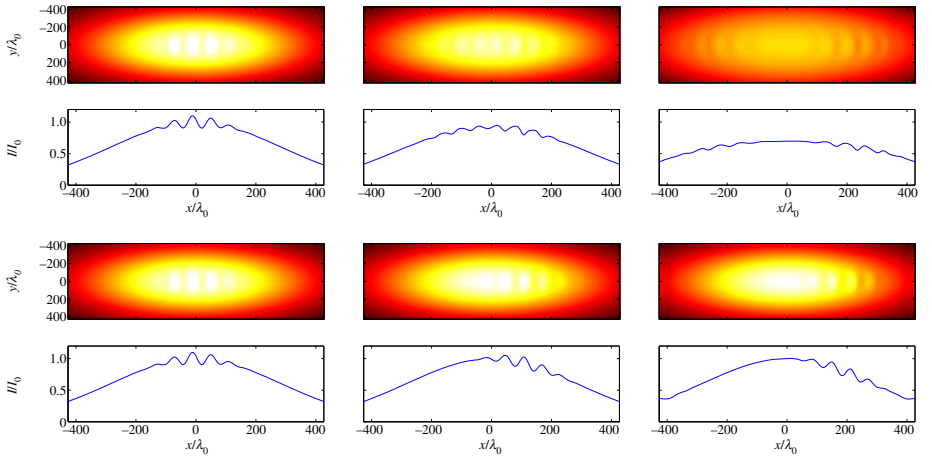

Figure 2. Propagation of weak excitations on top of a fluid of light at rest. The incident pump beam is normal to the front crystal interface. Its profile has a overall Gaussian shape with $w_g/\lambda_0 = 400$. The probe beam has the same frequency and a smaller Gaussian shape with $w_{pr}/\lambda_0 = 100$. It is incident on the front interface at a finite angle, corresponding to an in-plane wavevector $k_\perp^{pr}\lambda_0 = 0.1$ in the positive x-direction. The upper row shows a regime where the excitation is in the phonon regime ($k_\perp^{pr}\xi_0 = 0.56$); from left to right, the snapshots are for $z/\lambda_0 = 0$, 3000 and 7000. The bottom row shows a regime where the excitation is a single-particle one ($k_\perp^{pr}\xi \gg 1$); from left to right, the snapshots are for $z/\lambda_0 = 0$, 7000 and 12 000. On each row, the grey scale is normalized to the incident intensity. For each case, the lower panel shows a cut of the normalized intensity along the $y = 0$ line. In an experiment, one can go from the lower to the upper images by just increasing the pump intensity. (Online version in colour.)

parameter, the generated excitation will have a collective phonon (top row in the figure) or single-particle (bottom row) character. In practice, $k_\perp^{pr}\xi$ can be varied by tuning either the incidence angle ϕ_{pr} of the probe or the intensity $I_0 = |E_0|^2$ of the main pump. In figure 2, we adopt the latter strategy. For $k_\perp^{pr}\xi \ll 1$ (top row), both components are visible at long times as two separated wavepackets, symmetrically located with respect to $x = 0$. For $k_\perp^{pr}\xi \gg 1$ (bottom row), the very small weight of the hole component of the Bogoliubov mode makes the amplitude of the backward component at $\mathbf{q} = -\mathbf{k}_\perp^{pr}$ to be much smaller than the forward propagating one and practically invisible on the scale of the figure. A related experiment with ultracold atoms was reported in [19].

4. Suppressed scattering from a localized defect

One of the most important consequences of superfluidity is the suppressed drag force felt by a moving impurity crossing the superfluid at slow speeds. In this section, we discuss how an optical analogue of superfluidity can be observed in the present context of fluids of light in a propagating geometry. Inspired from previous work on superfluid light in planar cavities [1–5,20] and in atomic BECs [21], we consider a fluid of light that is moving at a finite speed in the transverse direction and hits a cylindrical defect located around $\mathbf{r}_\perp = 0$. This flow configuration is obtained with a single pump laser: according to (2.3), the flow speed in the transverse plane is controlled by the incidence angle ϕ of the beam, while the speed of sound c_s^0 is controlled by the incident intensity value $|E_0|^2$ via (3.3). The defect is described as a Gaussian-shaped modulation of the linear dielectric constant of the form

$$\delta\epsilon(\mathbf{r}_\perp, z) = \delta\epsilon_{max} \exp\left(-\frac{r_\perp^2}{2\sigma^2}\right) \tag{4.1}$$

centred at $\mathbf{r}_\perp = 0$ and of spatial size σ.

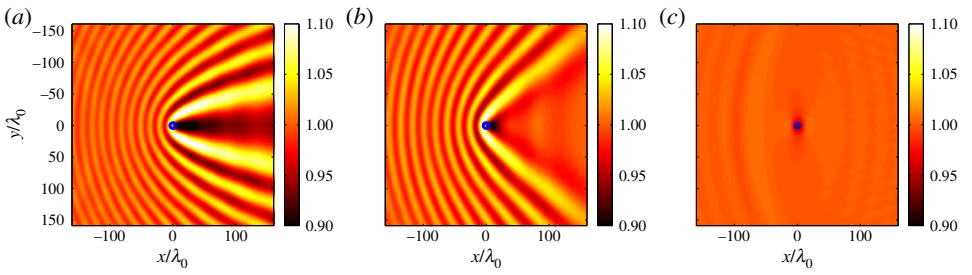

Figure 3. Long-distance asymptotic transverse profiles of the laser beam intensity hitting a cylindrical defect located at $\mathbf{r}_\perp = 0$. The flow velocity is the same $v = 0.034$ along the positive x-direction (the right-ward direction in the figure), while the light intensity is different in the three panels, increasing from left to right. The corresponding Mach numbers are $v/c_s^0 = \infty$ (linear optics limit, panel (*a*)), $v/c_s^0 = 1.84$ (supersonic flow regime, panel (*b*)), $v/c_s^0 = 0.86$ (superfluid regime, panel (*c*)). The defect parameters are $\sigma/\lambda_0 = 5$ and $\delta\epsilon_{\max}/\epsilon = -1.6 \times 10^{-4}$. The grey scale is normalized to the incident intensity. (Online version in colour.)

We begin our discussion from the weak defect regime where the small perturbation induced in the fluid can be described within a linearized Bogoliubov theory. Figure 3 illustrates the main regimes in the geometrically simplest case where the incident beam has a very wide profile. In this case, a $z \to \infty$ long-distance limit can be taken where the beam has already propagated for a very long distance and all transients have disappeared. Far from the defect, the light intensity profile recovers the incident intensity value $|E_0|^2$. The three panels refer to three different values of v/c_s^0: in the figure, we have chosen to keep v constant (that is the incidence angle) while varying c_s^0 (that is the light intensity). Of course, an identical physics would be observed if the incidence angle was varied at a fixed light intensity.

Figure 3*c* shows the superfluid regime $v < c_s^0$: the fluid of light moves at a subsonic speed and is able to flow around the defect without any friction. In the figure, this is visible in the absence of any intensity modulation far from the defect. In optical terms, it can be understood as the optical nonlinearity being able to effectively suppress the scattering of light from the cylindrical defect. On general grounds, one may expect that a suppressed scattering is associated to a suppressed radiation pressure acting on the defect: while this manuscript was under review, this intuitive picture has been theoretically confirmed in [22].

Figure 3*b* shows a supersonic flow regime where $v > c_s^0$ and superflow is broken: a Mach–Cerenkov cone appears downstream of the defect, with an aperture $\sin\theta = c_s^0/v$; in addition, parabolic-like precursors appear upstream of the defect. Figure 3*c* shows the extremely supersonic regime with $v \gg c_s^0$ that occurs in the linear optics regime at very low incident intensities: in this case, the linear interference of the incident and scattered light is responsible for parabolic shape of the fringes. A complete discussion of the rich features shown by the intensity modulation patterns in the different regimes can be found in the literature, in particular in [1,20,21,23]. Given the simple relation (2.3) between the incidence angle and the flow speed, the subsonic $v < c_s^0$ condition for superfluid flow translates in the present propagating geometry into an intensity-dependent upper bound on the (small) incidence angle

$$\phi < \sqrt{\epsilon} c_s^0 = \left[-\frac{\chi^{(3)}|E_0|^2}{2} \right]^{1/2}. \tag{4.2}$$

From an experimental perspective, the key parameter is therefore the maximum nonlinear refractive index shift $\delta n_{\max} = \chi^{(3)}|E_{\max}|^2/(2\sqrt{\epsilon})$ that can be obtained in the nonlinear medium before this is damaged: a larger $\delta n_{\max}$ allows for superfluidity at larger incidence angles and reduces the healing length ξ characterizing the spatial size of the spatial modulations. While working in the paraxial approximation does not pose special constraints on the numerical aperture of the optics to be used, having a larger critical angle for superfluidity would also

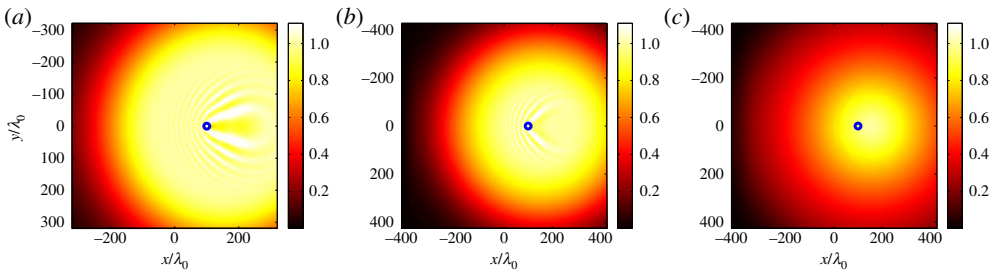

Figure 4. Transverse profiles of the laser beam intensity after a propagation distance $L/\lambda_0 = 4500$ in the nonlinear crystal. The incident beam has the flat-top intensity profile shown in figure 5*a* and a transverse carrier wavevector giving a flow velocity $v = 0.034$ along the positive x-direction. As in figure 3, the peak light intensity increases from left to right: panel (*a*) shows the linear optics regime with $v/c_s^0 \simeq \infty$, panel (*b*) shows the supersonic flow regime $v/c_s^0 = 1.88$, panel (*c*) shows the superfluid regime $v/c_s^0 = 0.77$. Same defect parameters as in figure 3. (Online version in colour.)

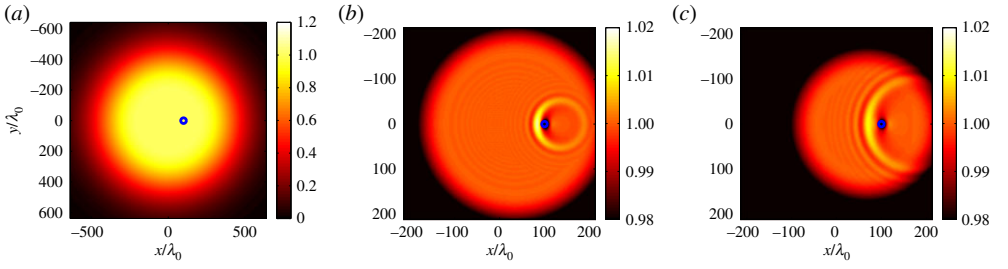

Figure 5. Panel (*a*) shows the transverse intensity profile of the flat-top incident laser beam: the inner flat region has a radius $w_f/\lambda_0 = 200$ and the Gaussian wings extend for $w_g/\lambda_0 = 300$. Panels (*b*,*c*) show the transverse intensity profiles after propagating for $L/\lambda_0 = 1000$ (centre) and 2000 (right). Same configuration as in figure 4*a*, but note the different grey scale. (Online version in colour.)

soften the lower bound on the pump spot size and therefore on the total laser power. As the superfluidity effect relies on the spatial modulation of the nonlinear refractive index shift, it is however important to choose a medium where the characteristic non-locality length is shorter than the healing length ξ. This feature is potentially most disturbing when using liquid nonlinear media [24].

Before proceeding, it is interesting to mention that light propagation in disordered systems with many random defects is presently the subject of intense studies, especially for what concerns the role of the optical nonlinearity on localization effects: in a qualitative agreement with our superfluidity picture, also in the disordered case, it appears that a defocusing nonlinearity tends to suppress the effect of the defects and therefore to destroy localization [25]. Following related advances in atomic gases [26], we expect that the many-body concepts discussed in this work will be of great utility to shine new light on the physics of light propagation in disordered systems.

Figure 4 illustrates how this physics is modified for realistic values of the crystal size and incident pump waist. In particular, we consider the flat-top incident beam of peak amplitude E_0 shown in figure 5*a*. As before, the super- or subsonic nature of the flow is defined according to the peak sound speed c_s^0 determined by inserting the peak intensity $|E_0|^2$ into (3.3). During propagation, the beam spot globally moves with speed v in the rightward direction, but also suffers some spatial expansion under the effect of the repulsive interactions. This latter effect is responsible for the apparently decreasing size of the high intensity region that one sees comparing figure 4*c* with the initial spot shown in figure 5*a*.

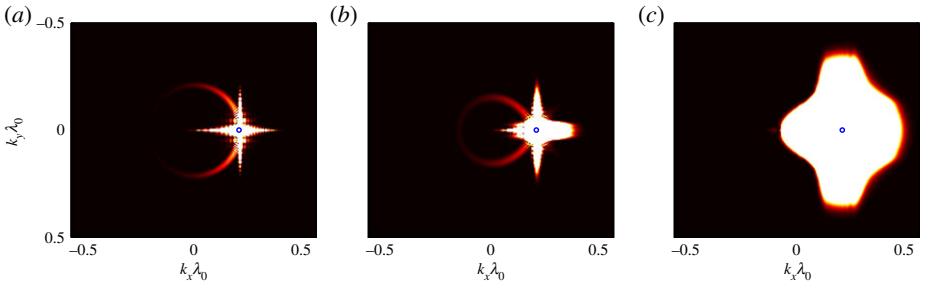

Figure 6. Far-field emission patterns for the same configurations as in figure 4 in a logarithmic grey scale. The circle indicates the incident wavevector $\mathbf{k}_\perp^{\mathrm{inc}}$. The wavevector $\mathbf{k}_\perp$ is related to the emission angle by $\sin\phi_{\mathrm{em}} = (k_\perp\lambda_0)\sqrt{\epsilon}/2\pi$. (Online version in colour.)

In the supersonic case shown in figure 4*a*,*b*, the main visible difference with respect to the corresponding panels of figure 3 is the finite spatial extension of the modulation pattern originating from the defect: the modulation starts forming as soon as light interacts with the defect and its spatial size keeps growing during propagation. At any given position, the modulation tends to a constant shape corresponding to the asymptotic pattern shown in figure 3.

In superfluid regime shown in figure 4*c* and, in more detail, in figure 5*b*,*c*, there is also a visible transient that propagates from the defect as a spherical wave. This wave is generated when the initially unperturbed Gaussian spot first hits the localized defect. While the whole spherical pattern drifts laterally as a consequence of the overall flow speed v, the radius of its inner rim grows at the speed of sound c_{s}^0 and shorter wavelength precursors expand at a faster rate as a consequence of the super-luminal nature of the Bogoliubov dispersion. Once the spherical wave has moved away from the defect, the intensity pattern tends to the asymptotic pattern shown in figure 3*c* which only shows a localized density dip at the defect location.

To complete the picture, it is interesting to display also $\mathbf{k}_\perp$-space profiles of the field amplitude that emerges from the back face of the crystal: these patterns are directly accessible in an experiment as the far-field angular pattern of the transmitted light (figure 6). In the strongly supersonic case $c_{\mathrm{s}}^0 \ll v$ shown in panel (*a*), scattering on the defect is responsible for a ring-shaped feature passing through the incident wavevector $\mathbf{k}_\perp^{\mathrm{inc}}$. When c_{s}^0 grows towards v, the ring is deformed developing a corner at $\mathbf{k}_\perp^{\mathrm{inc}}$ and a weaker copy of it appears at symmetric position with respect to $k_\perp^{\mathrm{inc}}$. This latter feature is another manifestation of the Bogoliubov transformation underlying the definition of the quasi-particle operators. In the $c_{\mathrm{s}}^0 > v$ superfluid regime shown in panel (*c*), the ring disappears and only a single peak at $\mathbf{k}_\perp^{\mathrm{inc}}$ remains visible: the strong broadening of this peak that is apparent in the figure is due to the overall rapid expansion of the spot under the effect of the repulsive interactions.

As it was originally predicted in the context of superfluid liquid Helium and recently experimentally observed in superfluids of light in planar cavities [3–5], more complex behaviours including the nucleation of solitons and vortices are observed for large and strong defects. First mentions of this physics in the optical context were given in [6,27]. A glimpse of this physics is given in figure 7 where some most significant examples of the spatial profile of the field after propagation in the nonlinear crystal are shown. For very low speeds, one would recover the superfluid behaviour already seen above (not shown). For intermediate speeds on the order of a fraction of c_{s}^0, pairs of vortices are continuously emitted by the defect (panel (*c*)). For large speeds $v > c_{\mathrm{s}}^0$ (panel (*a*)), the vortices tend to merge and eventually form a pair of oblique dark solitons.

5. Trans-sonic flows

In this section, I wish to briefly present a novel research axe where the remarkable properties of superfluid light in propagating geometries could be exploited to experimentally investigate aspects of quantum field theory on a curved space–time in a novel context.

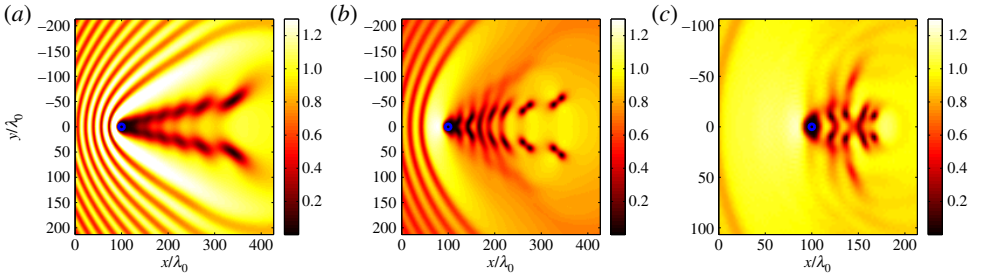

Figure 7. Transverse intensity profile of the beam after hitting a strong cylindrical defect with $\sigma/\lambda_0 = 4$ and $\delta\epsilon_{\max}/\epsilon = -0.03$ centred at $\mathbf{r}_\perp = 0$. The flow speed is the same $v = 0.034$ in the three panels, while the peak incident intensity grows from left to right, giving $v/c_s^0 = 2.66$ (*a*), $v/c_s^0 = 1.33$ (*b*) and $v/c_s^0 = 0.77$ (*c*). Propagation distance $z/\lambda_0 = 9500$ (*a*,*b*) and 4500 (*c*). Same flat top incident beam as in figure 4. (Online version in colour.)

Following the pioneering theoretical work in [28], the experiment [29] has recently demonstrated a trans-sonic flow configuration in a fluid of light: using a spatial constriction, an interface can be created in the flowing light which separates an upstream region of subsonic flow with $c_s > v$ from a downstream one of super-sonic flow $v > c_s$. As discussed at length in the literature on the so-called *analogue models* [30], the trans-sonic interface between the two regions shares close similarities with a black-hole horizon in gravitational physics.

Figure 8 illustrates how such flow configurations can be realized using a barrier-shaped refractive-index pattern of the form:

$$\delta\epsilon(\mathbf{r}_\perp, z) = \delta\epsilon_{\max} \exp\left(-\frac{(x - x_b)^2}{2\sigma^2}\right) \tag{5.1}$$

the modulation extends for the whole size of the crystal both along the propagation direction z and transversally along the y-direction, while the barrier has a finite thickness σ along x. Such patterns can be generated, e.g. via the nonlinear refractive index shift induced in a photo-refractive crystal by a light sheet, that is a light beam tightly focused along one direction only. For the incident pump, we consider a top-hat light beam focused on one side of the barrier with a small wavevector $\mathbf{k}_\perp^{\text{inc}}$ directed towards it. Its intensity profile is shown in the left panel: the quite unusual square flat-top shape was chosen in the calculations to suppress spurious features that would disturb the physics of interest. The other panels show the transverse intensity profile $|E(\mathbf{r}_\perp, z)|^2$ at different propagation distances z as obtained by a numerical solution of the Schrödinger equation (2.2).

As expected from the simulations for atomic condensates presented in [31], when the light fluid hits the barrier only a small part of it is transmitted, while the rest is reflected creating a series of planar fringes in front of the barrier. During propagation along the crystal, the planar fringes then form a dispersive shock wave, which is quickly expelled away from the barrier in the backward direction (central panels), eventually leaving regions of quite uniform density and speed on either side of the barrier (right panel). This very nonlinear phenomenon is to be contrasted to the linear optics regime where the barrier would reflect a sizable fraction of light creating a sinusoidal intensity modulation pattern in front of it.

The trans-sonic nature of the flow is visible in the cut displayed in the bottom panel: the solid line shows a cut of the local speed of sound along a line at constant $y = 0$ for the longest propagation distance considered in the figure: the curve was obtained inserting the numerically calculated intensity profile $|E(\mathbf{r}_\perp, z)|^2$ into the expression (3.3) for the speed of sound. The dashed line shows a cut along the same line of the x component of the local flow speed $\mathbf{v}$: given the field

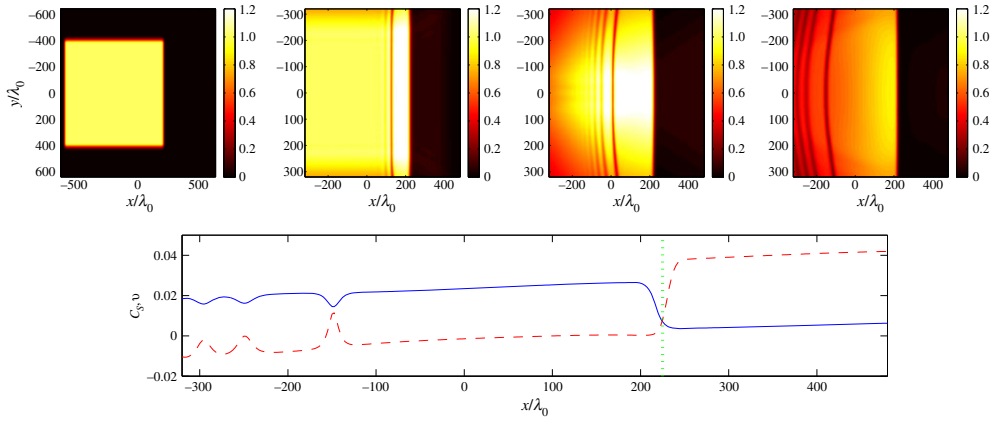

Figure 8. The upper row shows a few snapshots of the tranverse intensity profile for growing propagation distances from left to right: $z/\lambda_0 = 0$ (incident beam, left panel), 5000, 11 000 and 19 000 (right-most panel). The defect has a barrier shape, centred at $x_b/\lambda_0 = 225$ with $\delta\epsilon_{max}/\epsilon = -0.0016$ and $\sigma/\lambda_0 = 8$. The incident beam has $v/c_s^0 = 0.31$. In all panels, the grey scale is normalized to the incident intensity. The lower panel shows a cut along the $y = 0$ line of the local sound speed c_s (solid line) and of the x component of the local flow speed (dashed line) at the longest propagation distance $z/\lambda_0 = 19\,000$. The crossing point of the two curves in the vicinity of the barrier (vertical dotted line) indicates the position of the horizon. (Online version in colour.)

profile $E(\mathbf{r}_\perp, z)$, the local flow speed is obtained via

$$\mathbf{v}(\mathbf{r}_\perp, z) = \frac{1}{2ik_0|E(\mathbf{r}_\perp, z)|^2}[E^*(\mathbf{r}_\perp, z)\nabla_{\mathbf{r}_\perp}E(\mathbf{r}_\perp, z) - \text{h.c.}], \tag{5.2}$$

where the k_0 coefficient describes the photon mass as it appears in the Schrödinger equation (2.2). From the figure, it is apparent that after a sufficiently long propagation distance, the flow is subsonic $v < c_s$ upstream of the barrier (i.e. for $x < x_b$), while it is supersonic $v > c_s$ downstream of the barrier (i.e. for $x > x_b$): the barrier is indeed able to create a black hole horizon in the flowing fluid of light.

This has a lot of non-trivial consequences on light propagation. Following our previous work on analogue black holes in atomic condensates [32–34], we are presently addressing the hydrodynamic and quantum hydrodynamic properties of the horizon: scattering of a second probe beam off the horizon would provide a classical counterpart of the Hawking radiation, while correlations in the transmitted light would give evidence of the true Hawking emission originating from the conversion of zero-point fluctuations into observable phonons by the horizon. Along this route, a main conceptual issue [35] will be the development of a quantum theory of fluctuations that is able to deal with the propagating geometry, where the roles of space and time are mixed in a non-trivial way in the field equation.

6. Conclusion

In this article, we have reviewed how the concept of fluid of light can be used to shine new light on the classical problem of the paraxial propagation of a monochromatic laser beam in a Kerr nonlinear medium. Manifestations of superfluidity such as a suppressed scattering from defects in the medium are illustrated, as well as the generation of topological excitations such as solitons and defects. The perspectives of the propagating geometry for studies of analogue models of gravitational physics using fluids of light are finally outlined.

Acknowledgements. The research presented in this work builds on the long experience on superfluid light in planar microcavities that was accumulated during the years in collaboration with my numerous coauthors.

The more speculative study of trans-sonic flows in fluids of light has strongly benefitted from discussions with Stefano Finazzi, Daniele Faccio, Pierre-Élie Larré and Nicolas Pavloff.

Funding statement. This work was partially funded by ERC through the QGBE grant and by the Autonomous Province of Trento, Call *'Grandi Progetti 2012'*, project *'On silicon chip quantum optics for quantum computing and secure communications - SiQuro'*.

References

1. Carusotto I, Ciuti C. 2013 Quantum fluids of light. *Rev. Mod. Phys.* **85**, 299. (doi:10.1103/RevModPhys.85.299)
2. Amo A, Lefrère J, Pigeon S, Adrados C, Ciuti C, Carusotto I, Houdré R, Giacobino E, Bramati A. 2009 Superfluidity of polaritons in semiconductor microcavities. *Nat. Phys.* **5**, 805–810. (doi:10.1038/nphys1364)
3. Amo A *et al.* 2011 Polariton superfluids reveal quantum hydrodynamic solitons. *Science* **332**, 1167–1170. (doi:10.1126/science.1202307)
4. Nardin G, Grosso G, Leger Y, Pietka B, Morier-Genoud F, Deveaud-Pledran B. 2011 Hydrodynamic nucleation of quantized vortex pairs in a polariton quantum fluid. *Nat. Phys.* **7**, 635–641. (doi:10.1038/nphys1959)
5. Sanvitto D *et al.* 2011 All-optical control of the quantum flow of a polariton condensate. *Nat. Phot.* **5**, 610–614. (doi:10.1038/nphoton.2011.211)
6. Pomeau Y, Rica S. 1993 Nonlinear diffraction. In *Comptes Rendus de l'Academie des Sciences, Serie II*, vol. 317, p. 1287. Paris, France: Authier-Villars.
7. Wan W, Jia S, Fleischer JW. 2007 Dispersive superfluid-like shock waves in nonlinear optics. *Nat. Phys.* **3**, 46–51. (doi:10.1038/nphys486)
8. Wan W, Muenzel S, Fleischer JW. 2010 Wave tunneling and hysteresis in nonlinear junctions. *Phys. Rev. Lett.* **104**, 073903. (doi:10.1103/PhysRevLett.104.073903)
9. Jia S, Wan W, Fleischer JW. 2007 Dispersive shock waves in nonlinear arrays. *Phys. Rev. Lett.* **99**, 223901. (doi:10.1103/PhysRevLett.99.223901)
10. Wan W, Dylov DV, Barsi C, Fleischer JW. 2010 Diffraction from an edge in a self-focusing medium. *Opt. Lett.* **35**, 2819–2821. (doi:10.1364/OL.35.002819)
11. Jia S, Haataja M, Fleischer JW. 2012 Rayleigh-Taylor instability in nonlinear Schrödinger flow. *New J. Phys.* **7**, 075009. (doi:10.1088/1367-2630/14/7/075009)
12. Khamis EG, Gammal A, El GA, Gladush YuG, Kamchatnov AM. 2008 Nonlinear diffraction of light beams propagating in photorefractive media with embedded reflecting wire. *Phys. Rev. A* **78**, 013829. (doi:10.1103/PhysRevA.78.013829)
13. Leboeuf P, Moulieras S. 2010 Superfluid motion of light. *Phys. Rev. Lett.* **105**, 163904. (doi:10.1103/PhysRevLett.105.163904)
14. Nolte S, Will M, Burghoff J, Tuennermann A. 2003 Femtosecond waveguide writing: a new avenue to three-dimensional integrated optics. *Appl. Phys. A* **77**, 109–111. (doi:10.1007/s00339-003-2088-6)
15. Rechtsman MC, Zeuner JM, Plotnik Y, Lumer Y, Podolsky D, Dreisow F, Nolte S, Segev M, Szameit A. 2013 Photonic floquet topological insulators. *Nature* **496**, 196–200. (doi:10.1038/nature12066)
16. Jia S, Fleischer JW. 2009 Nonlinear light propagation in rotating waveguide arrays. *Phys. Rev. A* **79**, 041804(R). (doi:10.1103/PhysRevA.79.041804)
17. Pitaevskii LP, Stringari S. 2003 *Bose–Einstein condensation*. Oxford, UK: Clarendon Press.
18. Peyronel T, Firstenberg O, Liang Q-Y, Hofferberth S, Gorshkov AV, Pohl T, Lukin MD, Vuletić V. 2012 Quantum nonlinear optics with single photons enabled by strongly interacting atoms. *Nature* **488**, 57–60. (doi:10.1038/nature11361)
19. Vogels JM, Xu K, Raman C, Abo-Shaeer J-R, Ketterle W. 2002 Experimental observation of the Bogoliubov transformation for a Bose–Einstein condensed gas. *Phys. Rev. Lett.* **88**, 060402. (doi:10.1103/PhysRevLett.88.060402)
20. Carusotto I, Ciuti C. 2004 Probing microcavity polariton superfluidity through resonant rayleigh scattering. *Phys. Rev. Lett.* **93**, 166401. (doi:10.1103/PhysRevLett.93.166401)
21. Carusotto I, Hu SX, Collins LA, Smerzi A. 2006 Bogoliubov-Čerenkov radiation in a Bose–Einstein condensate flowing against an obstacle. *Phys. Rev. Lett.* **97**, 260403. (doi:10.1103/PhysRevLett.97.260403)

22. Larré P-É, Carusotto I. 2014 Optomechanical signature of a frictionless flow of superfluid light. (http://arxiv.org/abs/1405.2275)
23. Carusotto I, Rousseaux G. 2013 The Čerenkov effect revisited: from swimming ducks to zero modes in gravitational analogs. In *Analogue gravity phenomenology* (eds D Faccio, F Belgiorno, S Cacciatori, V Gorini, S Liberati, U Moschella), pp. 109–144. Heidelberg, Germany: Springer.
24. Bar-Ad S, Schilling R, Fleurov V. 2013 Nonlocality and fluctuations near the optical analog of a sonic horizon. *Phys. Rev. A* **87**, 013802. (doi:10.1103/PhysRevA.87.013802)
25. Segev M, Silberberg Y, Christodoulides DN. 2013 Anderson localization of light. *Nat. Photonics* **7**, 197–204. (doi:10.1038/nphoton.2013.30)
26. Sanchez-Palencia L, Lewenstein M. 2010 Disordered quantum gases under control. *Nat. Phys.* **6**, 87–95. (doi:10.1038/nphys1507)
27. Vaupel M, Staliunas K, Weiss CO. 1996 Hydrodynamic phenomena in laser physics: modes with flow and vortices behind an obstacle in an optical channel. *Phys. Rev. A* **54**, 880. (doi:10.1103/PhysRevA.54.880)
28. Fouxon I, Farberovich OV, Bar-Ad S, Fleurov V. 2010 Dynamics of fluctuations in an optical analogue of the Laval nozzle. *Europhys. Lett.* **92**, 14002. (doi:10.1209/0295-5075/92/14002)
29. Elazar M, Fleurov V, Bar-Ad S. 2012 An all-optical event horizon in an optical analogue of a Laval nozzle. *Phys. Rev. A* **86**, 063821. (doi:10.1103/PhysRevA.86.063821)
30. Barceló C, Liberati S, Visser M. 2005 Analogue gravity. *Living Rev. Relativ.* **8**, 12. (http://www.livingreviews.org/lrr-2005-12)
31. Kamchatnov AM, Pavloff N. 2012 Generation of dispersive shock waves by the flow of a Bose–Einstein condensate past a narrow obstacle. *Phys. Rev. A* **85**, 033603. (doi:10.1103/PhysRevA.85.033603)
32. Carusotto I, Fagnocchi S, Recati A, Balbinot R, Fabbri A. 2008 Numerical observation of Hawking radiation from acoustic black holes in atomic Bose–Einstein condensates. *New J. Phys.* **10**, 103001. (doi:10.1088/1367-2630/10/10/103001)
33. Recati A, Pavloff N, Carusotto I. 2009 Bogoliubov theory of acoustic Hawking radiation in Bose–Einstein condensates. *Phys. Rev. A* **80**, 043603. (doi:10.1103/PhysRevA.80.043603)
34. Larré P-É, Recati A, Carusotto I, Pavloff N. 2012 Quantum fluctuations around black hole horizons in Bose–Einstein condensates. *Phys. Rev. A* **85**, 013621. (doi:10.1103/PhysRevA.85.013621)
35. Elazar M, Bar-Ad S, Fleurov V, Schilling R. 2013 An all-optical event horizon in an optical analogue of a laval nozzle. In *Analogue gravity phenomenology* (eds D Faccio, F Belgiorno, S Cacciatori, V Gorini, S Liberati, U Moschella), pp. 275–296. Heidelberg, Germany: Springer.